JACS
JOURNAL OF THE AMERICAN CHEMICAL SOCIETY
Article
pubs.acs.org/JACS

Lithium–Sulfur Battery Cathode Enabled by Lithium–Nitrile Interaction

Juchen Guo,*[,†,§,∥] Zichao Yang,[†,∥] Yingchao Yu,[‡] Héctor D. Abruña,[‡] and Lynden A. Archer*[,†]

[†]School of Chemical and Biomolecular Engineering, and [‡]Department of Chemistry and Chemical Biology, Cornell University, Ithaca, New York 14853, United States

Supporting Information

ABSTRACT: Lithium sulfide is a promising cathode material for high-energy lithium ion batteries because, unlike elemental sulfur, it obviates the need for metallic lithium anodes. Like elemental sulfur, however, a successful lithium sulfide cathode requires an inherent mechanism for preventing lithium polysulfide dissolution and shuttling during electrochemical cycling. A new scheme is proposed to create composites based on lithium sulfide uniformly dispersed in a carbon host, which serve to sequester polysulfides. The synthesis methodology makes use of interactions between lithium ions in solution and nitrile groups uniformly distributed along the chain backbone of a polymer precursor (e.g., polyacrylonitrile), to control the distribution of lithium sulfide in the host material. The Li_2S–carbon composites obtained by carbonizing the precursor are evaluated as cathode materials in a half-cell lithium battery, and are shown to yield high galvanic charge/discharge capacities and excellent Coulombic efficiency, demonstrating the effectiveness of the architecture in homogeneously distributing Li_2S and in sequestering lithium polysulfides.

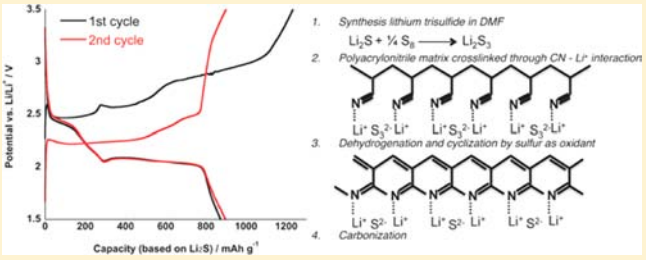

INTRODUCTION

A rechargeable lithium–sulfur (Li–S) battery is based on the reversible oxidization–reduction reaction between sulfur and lithium. The Li–S battery platform is currently under intensive investigation by research groups worldwide because of its promise for low-cost, high-energy electrochemical storage. Conventional Li–S batteries used elemental sulfur (with conductive additives) as the cathode, an aprotic liquid electrolyte, and lithium metal as the anode. Loss of active materials and the shuttle reaction induced by lithium polysulfide dissolution in the electrolyte presented significant challenges. To sequester the lithium polysulfide, the most frequently adopted current strategy is to incorporate sulfur into carbon hosts with porous structure and/or high aspect ratio, such as carbon nanotubes,[1−5] graphene/graphene oxide sheets,[6−10] and mesoporous carbon structures.[11−16]

The ideal configuration for a sulfur–carbon cathode is to have uniform and high sulfur dispersion, complete sulfur enclosure in a confined, but accessible space, and strong sulfur–host affinity to achieve high capacity (in-depth sulfur utilization) and excellent capacity retention.[17] Current synthesis methods do not meet this goal for a variety of reasons: First, in most cases, the carbon host materials are pre-existing or preprepared. The ex situ infusion of sulfur into such a host is limited by the host structure and surface chemistry, and, as a result, generally cannot ensure uniform sulfur distribution in the host. Second, despite the very small pore sizes (<5 nm) that can be achieved in some carbon materials, the modest Coulombic efficiencies of Li–S cells indicate that some lithium polysulfides may still leach out (e.g., by an analogous process to liquid sulfur infusion) or be extracted from the host by the electrolyte. Therefore, the physical barriers to polysulfide loss provided by carbon sequestration and adsorption can, at best, only be expected to slow the dissolution. Finally, to date only limited evidence has been reported on the role specific chemical interactions between sulfur and the host materials might play in ensuring uniform distribution and good sequestration. The exceptions are a few studies that indicate an association between sulfur and amorphous carbon and between sulfur and graphene oxide might stabilize the sulfur.[1,6] New sulfur synthesis routes can provide multiple potential strategies for overcoming these problems.

In this Article, we report a novel route toward lithium sulfide–carbon composite cathodes. Lithium sulfide (Li_2S), the fully lithiated sulfur product, is already under active investigation for its promise as a cathode.[18−20] Because the cathode is lithiated, it can be paired with high capacity anode materials other than metallic lithium. Also, unlike sulfur that sublimes at a modest temperature, Li_2S has a high decomposition temperature above 900 °C, which improves its processing in carbon composites. The particular property of Li_2S we utilize in our synthesis is the capacity of the lithium ions to strongly interact with electron-donating groups in carbon-precursor polymers such as polyacrylonitrile (PAN). Specifically, lone pair electrons in the nitrile group of PAN are

Received: September 26, 2012
Published: December 12, 2012

   dx.doi.org/10.1021/ja309435f | J. Am. Chem. Soc. 2013, 135, 763–767

capable of interacting with lithium through a coordination bond-like interaction. Thus, when lithium sulfide is mixed with PAN in a homogeneous solution, Li_2S may function as a cross-linking agent, which interconnects the PAN network via lithium sulfide net-nodes. We hypothesize that, in addition to stiffening the PAN framework, such linkages favor uniform dispersion of Li_2S in the PAN matrix. We show that the resultant lithium sulfide−PAN cross-linked matrix can be carbonized at elevated temperature in an inert environment to obtain an ideal Li_2S−C composite cathode material in which Li_2S is uniformly and completely dispersed in carbon.

RESULTS AND DISCUSSION

The specific synthesis route used in the study is shown in Scheme 1 and detailed in the experimental section (see the Supporting Information). The method takes advantage of the easy conversion of Li_2S to Li_2S_x, to create a dimethylformamide (DMF)-soluble Li_2S_3 salt. Because DMF is a good solvent for PAN, codissolution of the Li_2S_3 salt and PAN promotes uniform dispersion in a high-dielectric constant DMF medium, which favors ion pair dissociation of Li_2S_3 and cross-linking of the polymer in solution.

Scheme 1. Proposed Synthesis Route for Creating Li_2S−Carbon Cathode Materials

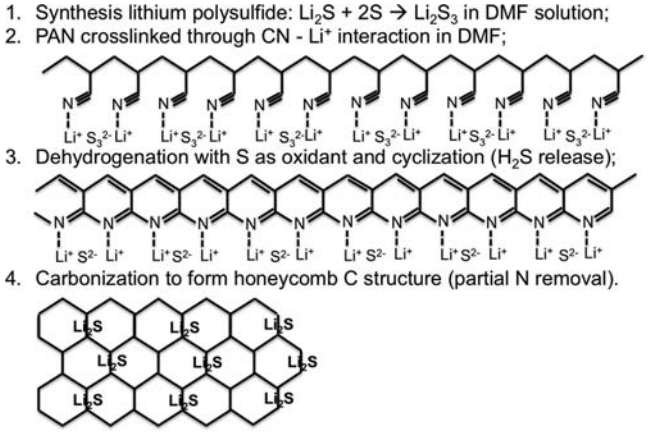

To prepare Li_2S_3−PAN composites, the cross-linked polymer was first treated at 100 °C for 48 h under vacuum to remove the DMF. The resultant solid material was pulverized by mechanical ball milling to yield a fine powder, which was heated in an argon-filled furnace at 300 °C for 2 h. As shown in Scheme 1, two simultaneous reactions are thought to occur in this step: The first is cyclization in which one of the triple bonds in the nitrile group cleaves, and the nitrogen sequentially bonds to the carbon in the neighboring nitrile group, thus forming ring-like structures. This reaction is accompanied by dehydrogenation in which Li_2S_3 decomposes to yield Li_2S and elemental sulfur, which is lost as H_2S, by combining with the hydrogen atoms in the PAN chain. Dehydrogenation and cyclicization of PAN in the presence of sulfur has been reported previously.[21−23] After heat treatment at 300 °C, the material was further maintained in an argon atmosphere at 600 °C for 30 min to carbonize the PAN. On the basis of the proposed mechanism, the Li_2S−C composite formation could result in N-containing carbon (ring) structures encapsulating lithium sulfide species. It is noteworthy that, although Li_2S is hygroscopic, Li_2S_3 is stable under ambient conditions, and therefore the cross-linking reaction and the drying processes can be performed in ambient air outside the glovebox.

After carbonization, the product in the form of a fine black powder was characterized by X-ray diffraction (XRD, Scintag Theta−Theta X-ray diffractometer) and compared to the vacuum-dried cross-linked Li_2S_3−PAN composite, as well as the material after dehydrogenation at 300 °C. The XRD results for these three materials are shown in Figure 1. The Li_2S_3−PAN composite is clearly seen to be in an amorphous state, which is consistent with the fact that lithium polysulfides are chemical compounds with stoichiometric lithium/sulfur ratios, without crystalline structure. The XRD patterns in Figure 1b and c can be unambiguously assigned to the Li_2S phase (JCPDS card no. 23-0369), clearly showing that Li_2S is produced in the composite after the dehydrogenation step. This is expected due to Li_2S_3 decomposition, as shown in Figure 1b. The weight fraction of Li_2S can be determined from oxidative TGA, with the TGA curve provided as Supporting Information, Figure S1. Assuming complete oxidization of the carbon and complete conversion from Li_2S (molar mass 45.95 g mol^{-1}) to Li_2SO_4 (molar mass 109.94 g mol^{-1}), based on the final weight gain percentage (124 wt %) of the Li_2S−C after TGA, the Li_2S weight ratio in the Li_2S−C composite is calculated to be 51.8 wt %. The XRD pattern of the material remaining after TGA analysis is shown in Supporting Information Figure S2, which can be assigned to Li_2SO_4 (JCPDS card no. 20-0640).

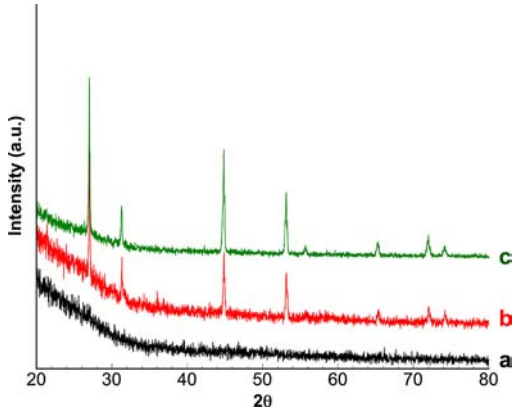

Figure 1. XRD patterns for (a) cross-linked Li_2S_3−PAN after vacuum drying; (b) Li_2S_3−PAN after heat treatment (dehydrogenation and cyclization) at 300 °C; and (c) Li_2S−C after carbonization at 600 °C.

Infrared spectra of Li_2S−C composites synthesized at 300 and 600 °C, PAN carbonized at 600 °C for 2 h, and bulk Li_2S are provided as Supporting Information, Figure S3. The nitrile stretch (2240−2260 cm^{-1}) is absent in all samples, which is consistent with the fact that nitrile groups do not exist in heat-treated PAN. The IR peak at 1560 cm^{-1} in the carbonized PAN can be assigned to the C═N stretch, which is a signature of C═N groups formed during the cyclization of PAN. This peak is noticeably shifted to 1430 cm^{-1} with an emerging shoulder at approximately 1500 cm^{-1} in the Li_2S−C composites processed at 300 and 600 °C. This shift is attributed to interactions between the nitrogen atoms and the lithium salt. The IR peaks in the range of 1150−1300 cm^{-1} are assigned to the stretching modes of the C−N bond. These peaks also show different patterns in the three materials (PAN carbon, Li_2S−C 300 °C, and Li_2S−C 600 °C), which are also consistent with the

dx.doi.org/10.1021/ja309435f | J. Am. Chem. Soc. 2013, 135, 763−767

presence of local interactions between nitrogen and the lithium salts.

Raman spectra of the Li_2S–C composites synthesized at 300 and 600 °C are reported in Supporting Information Figure S4a, along with spectra for PAN carbonized at 600 °C for 2 h and the glass holder used. Raman spectra for the Li_2S–C composites and carbonized PAN all contain bands corresponding to graphite (G), disordered graphitic lattices (D1), and amorphous carbon (D3),[24,25] as seen in the deconvoluted spectrum in Figure S4b and c. This indicates the partially graphitic nature of PAN carbonized under the conditions used in the study. The wavenumbers, band half widths, and relative areas of the deconvoluted peaks are provided in Table S1. It is seen that the Li_2S composite has lower graphitic content, as compared to pure PAN carbonized at the same temperature, which we interpret to be a result of associations between lithium sulfide and the carbon-chain backbone of PAN, which is thought to hinder formation of graphitic lattices during carbonization of the PAN.

Figure 2a shows a typical TEM image of the Li_2S–C composite carbonized at 600 °C, indicating the formation of flake-like structures. Similar structures have been observed in the literature for carbonized PAN.[26,27] To determine the distribution of lithium sulfide in the composite, elemental identification is performed on the 600 °C Li_2S–C composite. Figure 2c and d shows the energy dispersive X-ray (EDX) maps for carbon and sulfur based on the area shown in the annular dark field (ADF) image (Figure 2b). The edge of carbon and sulfur EDX maps in Figure 2c and d matches the result shown in the ADF image, indicating that carbon and sulfur are homogeneously distributed throughout the composite. Because the K edge of lithium (55 eV) is not detectable using EDX, electron energy loss spectroscopy (EELS) was performed on the composite to investigate the presence of lithium. Figure 2e reports a line scan of normalized EELS intensities, with respect to position for Li–K edge, S-$L_{2,3}$ edges, and C–K edge shown in Figure 2f. The results demonstrate that, in addition to carbon and sulfur, lithium is also uniformly dispersed in the composite material (the EDX spectrum and original and power-law background subtracted EELS data are found in Supporting Information Figure S5). These observations support our hypothesis that by making use of Li–N interactions, Li_2S–C composites in which lithium and sulfur are uniformly dispersed in carbon can be obtained.

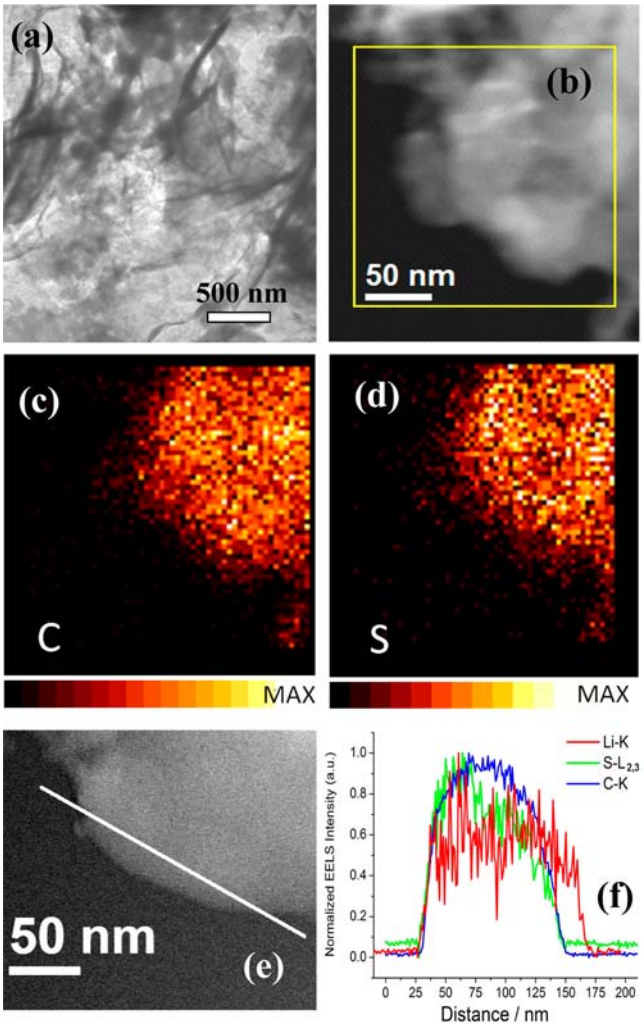

Figure 2. TEM (a) and STEM (b) images of the Li_2S–C composite; (c and d) EDX carbon and sulfur maps based on the area shown in (b); and (e) STEM image and (f) normalized EELS intensity along the line in (e).

The electrochemical properties of the Li_2S–C composites were characterized in coin cells with the composite as the cathode and lithium foil as the counter electrode. Figure 3 shows the first three cyclic voltammetry (CV) cycles of the Li_2S–C cathode vs Li/Li^+ from 1.5 to 3.5 V at a scanning rate of 0.05 mV s^{-1}. Because the Li_2S–C material is lithiated, the CV measurements were started with a delithiation process created by increasing the potential from the open circuit potential. The first cathodic peak is seen to be broad and centered at 3.1 V with a small shoulder at 2.75 V. The potential of this cathodic peak is distinctly higher than the cathodic peaks from conventional S–C cathode materials, which are typically seen at approximately 2.5 V. The higher cathodic peak of the Li_2S–C composite indicates a delithiation reaction with higher energy barrier than that seen in conventional S–C cathodes. It could be reflective of the Li–N bonding from the nitrogen containing groups in the carbon. After the delithiation, the first anodic scan shows typical sulfur-oxidizing-Li CV peaks at 2.35, 2.1, and 1.9 V. The second cathodic scan shows a major cathodic peak at 2.55 V, which is more consistent with the conventional S–C cathodes. Also, the amplitude of the broad cathodic peak at 3.1 V is greatly reduced. The third CV cycle displays a more pronounced cathodic peak at 2.55 V and

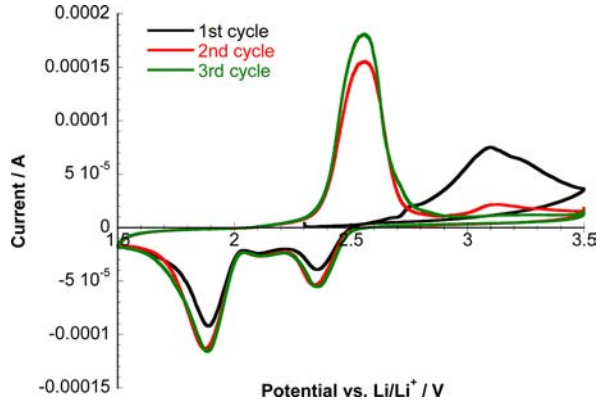

Figure 3. Cyclic voltammograms of the as-prepared Li_2S–C composite cathodes at a scan rate of 0.05 mV/s.

dx.doi.org/10.1021/ja309435f | J. Am. Chem. Soc. 2013, 135, 763–767

absence of the 3.1 V cathodic peak. The anodic peaks remain stable and consistent. The evolution of the CV curves at different cycles is consistent with our hypothesis that the Li_2S–C cathode material is enabled by the Li–N bonding, which produces the unusual high potential delithiation reaction in the initial cycles. As illustrated in Figure S6, Supporting Information, CV cycling started with lithiation (decreasing potential from OCP vs Li/Li^+) showed the same mechanism.

Galvanostatic charge/discharge measurements were also used to characterize the Li_2S–C composite cathodes. These measurements reveal an unusual delithiation reaction in the Li_2S–C cathode as shown in Figure 4. To minimize the effect

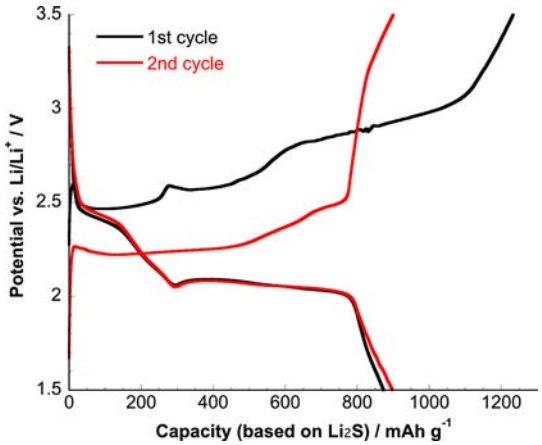

Figure 4. The first two galvanostatic charge/discharge profiles of the Li_2S–C cathode at a low charge/discharge rate of 10 mA g^{-1}. These measurements are designed to characterize the near-equilibrium state electrochemical performance of the cathode.

of any transport barriers, leading to an overpotential, the Li_2S–C cathode was charged and discharged at a very low current density at 10 mA g^{-1}, based on the mass of active material Li_2S (51.8% of total mass). The first charging curve suggests that there are three plateaus, that is, three delithiation steps in the first charging process. The first plateau at 2.5 V and the second at approximately 2.75 V are followed by a regime in which the potential gradually increases to between 2.8 and 3.0 V. Because the galvanostatic measurements were performed under a very slow rate (~110 h charging time vs ~11 h charging time in CV), the electrochemical reactions are considered to take place under conditions that approach thermodynamic equilibrium. Therefore, the higher delithiation potential in the first charge is real and appears to be truly an indication of a higher energy barrier induced by the Li–N bonding. The subsequent cycling process demonstrated discharge/charge profiles consistent with the conventional sulfur cathode, and a reversible capacity of approximately 900 mAh g^{-1} (based on the active material mass in the electrode) was achieved, which is close to the theoretical capacity of Li_2S (1166 mAh g^{-1}). Figure 5 reports the stability and Coulombic efficiency of the Li_2S–C cathode under a charge/discharge current of 200 mA g^{-1} based on Li_2S. Stable reversible capacities of 500 mA g^{-1} and Coulombic efficiencies of nearly 100% were achieved, indicating the effectiveness of the dispersed Li_2S architecture in sequestering sulfur and inhibiting shuttling reaction.

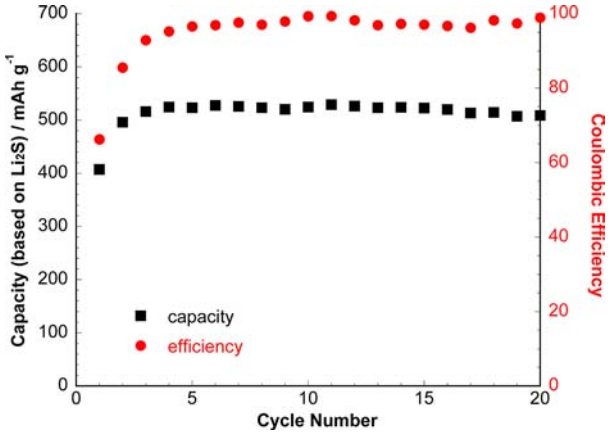

Figure 5. Discharge capacity (left axis) and Coulombic efficiency (right axis) of the Li_2S–C cathode as a function of cycle number. A fixed current density of 200 mA g^{-1} was used for these measurements.

CONCLUSION

We have shown that interactions between lithium ions and nitrile groups in a high-molar mass polyacrylonitrile (PAN) can be used to create carbon–Li_2S composites in which Li_2S is uniformly distributed in a carbon host. We believe that similar approaches can be used to control the distribution of other metal salts in polymer- or carbon-based composites. Preliminary results indicate that carbon–Li_2S composites created using the new approach offer superior potential, in comparison to other reported methods, as cathode materials for high-energy lithium ion batteries with great cycling stability and excellent Coulombic efficiency. The improved performance of the new composite cathodes can be attributed to the uniform dispersion of Li_2S in carbon and the ability of the structures to sequester higher order polysulfides generated during electrochemical cycling. Although more work is needed to fundamentally understand the details of the bonding between lithium and nitrile groups in PAN, the current study shows that Li_2S_x is an efficient cross-linker for PAN in solvents such as DMF with high dielectric constants. This suggests that a coordination-like interaction between Li^+ ions in solution and nitrogen atoms along the polymer backbone is responsible for the uniform dispersion of Li_2S achieved in the composites.

ASSOCIATED CONTENT

Supporting Information

Experimental details for the preparation of the lithium sulfide composite cathode, materials characterization, and electrochemical characterization. This material is available free of charge via the Internet at http://pubs.acs.org.

AUTHOR INFORMATION

Corresponding Author

laa25@cornell.edu; jguo@engr.ucr.edu

Present Address

[§]Department of Chemical and Environmental Engineering, University of California at Riverside, Riverside, California 92521, United States.

Author Contributions

[‖]These authors contributed equally.

Notes

The authors declare the following competing financial interest(s): Professor Archer is the co-founder and holds a

financial interest in NOHMs Technologies, a technology concern focused on commercialization of electrodes and electrolytes for Li/S secondary batteries.

■ ACKNOWLEDGMENTS

This material is based on work supported in part by the Energy Materials Center at Cornell, an Energy Frontier Research Center funded by the U.S. Department of Energy, Office of Science, Office of Basic Energy Sciences under Award Number DESC0001086. We also acknowledge the National Science Foundation, Partnerships for Innovation Program (Grant no. IIP-1237622) for partial support of the study. Y.Y. acknowledges the fellowship from ACS Division of Analytical Chemistry and support from Eastman Chemical Co. This work made use of the electron microscopy facility at the Cornell Center for Materials Research, a NSF supported MRSEC through Grant DMR-1120296.

■ REFERENCES

(1) Guo, J.; Xu, Y.; Wang, C. *Nano Lett.* **2011**, *11*, 4288.
(2) Zheng, G.; Yang, Y.; Cha, J. J.; Hong, S. S.; Cui, Y. *Nano Lett.* **2011**, *11*, 4462.
(3) Dorfler, S.; Hagen, M.; Althues, H.; Tubke, J.; Kaskel, S.; Hoffmann, M. *Chem. Commun.* **2012**, *48*, 4097.
(4) Su, Y.; Manthiram, A. *Chem. Commun.* **2012**, *48*, 8817.
(5) Zhou, G.; Wang, D.; Li, F.; Hou, P.; Yin, L.; Liu, C.; Lu, G.; Gentle, I. R.; Cheng, H. *Energy Environ. Sci.* **2012**, *5*, 8901.
(6) Ji, L.; Rao, M.; Zheng, H.; Zhang, L.; Li, Y.; Duan, W.; Guo, J.; Cairns, E. J.; Zhang, Y. *J. Am. Chem. Soc.* **2011**, *133*, 18522.
(7) Wang, H.; Yang, Y.; Liang, Y.; Robinson, J. T.; Li, Y.; Jackson, A.; Cui, Y.; Dai, H. *Nano Lett.* **2011**, *11*, 2644.
(8) Cao, Y.; Li, X.; Aksay, I. A.; Lemmon, J.; Nie, Z.; Yang, Z.; Liu, J. *Phys. Chem. Chem. Phys.* **2011**, *13*, 7660.
(9) Wei, Z.; Chen, J.; Qin, L.; Nemage, A.; Zheng, M.; Dong, Q. *J. Electrochem. Soc.* **2012**, *159*, A1236.
(10) Li, N.; Zheng, M.; Lu, H.; Hu, Z.; Shen, C.; Chang, X.; Ji, G.; Cao, J.; Shi, Y. *Chem. Commun.* **2012**, *48*, 4106.
(11) Ji, X.; Lee, K.; Nazar, L. F. *Nat. Mater.* **2009**, *8*, 500.
(12) Liang, C.; Dudney, N. J.; Howe, J. Y. *Chem. Mater.* **2009**, *21*, 4724.
(13) Zhang, B.; Qin, X.; Li, G. R.; Gao, X. P. *Energy Environ. Sci.* **2010**, *3*, 1531.
(14) Jayaprakash, N.; Shen, J.; Moganty, S. S.; Corona, A.; Archer, L. A. *Angew. Chem., Int. Ed.* **2011**, *50*, 5904.
(15) Ji, X.; Evers, S.; Black, R.; Nazar, L. F. *Nat. Commun.* **2011**, *2*, 1.
(16) Zhang, C.; Wu, H.; Yuan, C.; Guo, Z.; Lou, X. *Angew. Chem., Int. Ed.* **2012**, *51*, 9592.
(17) Xiao, L.; Cao, Y.; Xiao, J.; Schwenzer, B.; Engelhard, M. H.; Saraf, L. V.; Nie, Z.; Exarhos, G. J.; Liu, J. *Adv. Mater.* **2012**, *24*, 1176.
(18) Yang, Y.; McDowell, M. T.; Jackson, A.; Cha, J. J.; Hong, S.; Cui, Y. *Nano Lett.* **2010**, *10*, 1486.
(19) Hassoun, J.; Scrosati, B. *Angew. Chem., Int. Ed.* **2010**, *49*, 2371.
(20) Yang, Y.; Zheng, G. Y.; Misra, S.; Nelson, J.; Toney, M. F.; Cui, Y. *J. Am. Chem. Soc.* **2012**, *134*, 15387.
(21) Wang, J.; Yang, J.; Xie, J.; Xu, N. *Adv. Mater.* **2002**, *14*, 963.
(22) Wang, J.; Yang, J.; Wan, C.; Du, K.; Xie, J.; Xu, N. *Adv. Funct. Mater.* **2003**, *13*, 487.
(23) Yu, X. G.; Xie, J. Y.; Li, Y.; Huang, H. J.; Lai, C. Y.; Wang, K. *J. Power Sources* **2005**, *146*, 335.
(24) Sadezky, A.; Mukenhuber, H.; Grothe, H.; Niessner, R.; Poschl, U. *Carbon* **2005**, *43*, 1731.
(25) Kim, C.; Park, S.-H.; Cho, J.-I.; Lee, D.-Y.; Park, T.-J.; Lee, W.-J.; Yang, K. S. *J. Raman Spectrosc.* **2004**, *35*, 928.
(26) Lai, C.; Gao, X. P.; Zhang, B.; Yan, T. Y.; Zhou, Z. *J. Phys. Chem. C* **2009**, *113*, 4712.
(27) Wang, G.; Ma, Y. Q.; Liu, Z. Y.; Wu, J. N. *Electrochim. Acta* **2012**, *65*, 275.